PALS Approach to Study of Water–Adsorption Processes in Nanostructured $MgAl_2O_3$ Ceramics: From Three- to Four-Component Fitting Procedures

H. Klym

1 Introduction

A long time nanostructured $MgAl_2O_4$ ceramics are interesting materials for humidity sensors due to their inner nanoporous structure and surface porosity, which promotes effective cooperative adsorption of water molecular [1–4]. The humidity-sensing application of these ceramics is known to be determinant of chemical and physical water–adsorption processes occurring within inner pores in ceramics bulk [5–7]. The presence of open porosity permits greater conductivity due to the enhancement of the specific surface area available for water–adsorption [8–10]. Recently, it was shown that amount of adsorbed water in these ceramics affects not only their electrical conductivity, but also other physical–chemical parameters [10, 11]. Such parameters can be the positron trapping modes of free volumes (or nanovoids) studied by positron annihilation lifetime spectroscopy (PALS)—one of the most informative experimental methods for studying of structurally intrinsic nanovoids in solids such as ceramics [12–15], thick films based on ceramics [15–17], and nanocomposites [18, 19] in the form of different modifications (clusters, agglomerates, nanopores, etc.) [20, 21].

We have achieved significant success in the study of spinel $MgAl_2O_4$ ceramics by the PALS method [8, 10, 11, 21]. It was shown that positrons injected in the studied $MgAl_2O_4$ ceramics can undergo two different processes such as positron trapping and ortho-positronium o-Ps decaying. The latter process (so-called "pick-off" annihilation) resulting from Ps interaction with electron from environment (including annihilation in liquid water) is ended by emission of two γ-quanta [20, 22]. In general, these two channels of positron annihilation are independent. However, if trapping sites will appear in a vicinity of grain boundaries neighboring with free-volume

H. Klym (✉)
Lviv Polytechnic National University, S. Bandery Str., 12, Lviv 79013, Ukraine
e-mail: halyna.i.klym@lpnu.ua

O. Fesenko and L. Yatsenko (eds.), *Nanomaterials and Nanocomposites, Nanostructure Surfaces, and Their Applications*, Springer Proceedings in Physics 263, https://doi.org/10.1007/978-3-030-74741-1_24

pores, these positron-positronium traps become mutually interconnected resulting in a significant complication of PALS data.

We have developed several approaches to the analysis of PALS spectra for the humidity-sensitive $MgAl_2O_4$ ceramics using different numbers of fitting parameters and algorithms to justify the obtained results [21, 23–25]. The goal of this work is to generalize in one work the previously presented approaches to the analysis of the PALS spectra of nanostructured spinel-type $MgAl_2O_4$ ceramics at adsorption of water. The trapping of PALS spectra is presented at the analysis on three and four components and also at the fixed values of some positron trapping parameters.

2 Sample Preparation and Experimental

The studied spinel-type $MgAl_2O_4$ ceramics were sintered from fine-dispersive Al_2O_3 and MgO powders using a special regime with maximal temperatures T_s of 1400 °C, the total duration being 2 h [21, 23]. In a result, the humidity-sensitive ceramics with a so-called trimodal pore size distribution and character values of pore radiuses centered near ~0.003, 0.09 and 0.4 μm were obtained [21]. The phase composition of ceramics obtained with X-ray diffraction [21, 23] was established that the studied ceramics contained the main spinel phase and small quantity of MgO phase (1.5%).

PALS measurements were performed using an ORTEC spectrometer [20, 26]. The ^{22}Na isotope was used as positron source, placed between two identical samples. The obtained PALS spectra were decomposed by LT computer program of Kansy [27]. In this work, three experimental and analysis approaches were presented to study of water–adsorption processes in the nanostructured $MgAl_2O_4$ ceramics using PALS method.

The first approach: analysis of PALS spectra by three-component fitting procedure in $MgAl_2O_4$ ceramics before and after water–adsorption. PALS measurements were performed at 20 °C and ~35% relative humidity [21]. We used three measured PALS spectra for each investigated pair of samples, the best results being chosen by comparing statistically weighted least-squares deviations between experimental points and theoretical curve. In order to change interrelation between positron trapping and Ps decay modes in the deconvoluted PALS spectra, we placed the samples into distillated water for 12 h. Then, the PALS measurements were repeated once more with water-immersed $MgAl_2O_4$ ceramics at the same conditions. We used three-component fitting of PALS spectra and obtained fitting parameters (positron lifetimes τ_1, τ_2, τ_3 and corresponding unity-normalized intensities I_1, I_2, I_3). Typical PALS spectra decomposed on three components using LT program (with τ_1, τ_2 and τ_3 lifetimes as well as I_1, I_2, and I_3 intensities) are shown in Fig. 1.

The second approach: analysis of PALS spectra by three-component fitting procedure in the $MgAl_2O_4$ ceramics at fixation of the lifetimes of the first and the second PALS components within row of relative humidity (*RH*). PALS measurements were performed at 20 °C. The selection of corresponding values for measuring chamber

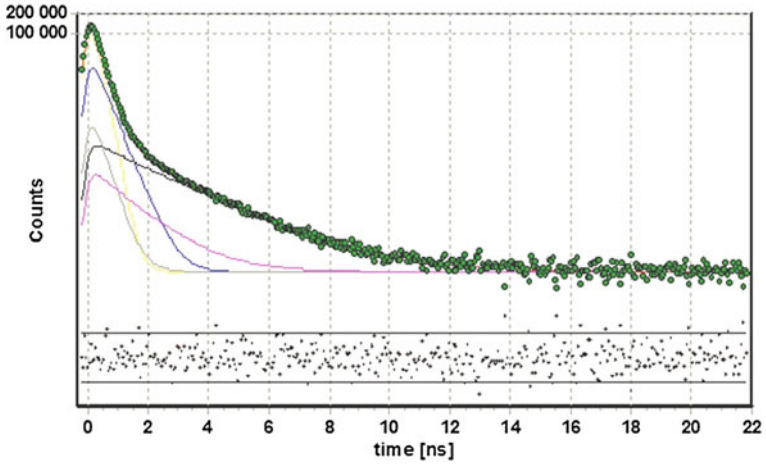

Fig. 1 Fitting of PALS spectra for $MgAl_2O_4$ ceramics on three components using LT computer program [28]

permit to investigation of samples at constant values of relative humidity in the range of 25–60% and 25–98% [24, 28].

Special testing procedure with a set of standard thermally treated non-defected Ni and Al probes was performed to correctly account for source input and other positron trapping channels in the measured lifetime spectra. The obtained data were mathematically treated at three-component fitting procedure with the fixed positron lifetimes of the first and second PALS components (τ_1 and τ_2). Only results with FIT (short abbreviation originated from "fitting") values close to 1.0 [24] were left for further consideration.

The third approach: analysis of PALS spectra by four-component fitting procedure in $MgAl_2O_4$ ceramics before and after water–adsorption [23]. The PALS measurements were performed at 22 °C and relative humidity RH = 35% after drying (initial samples) and after 7 days of water exposure (water vapor in desiccator at RH = 100%). Each PALS spectrum was collected within 6.15 ps channel width to analyze short and intermediate PALS components. To obtain data on longest-lived PALS components, the same ceramics were studied within a channel width of 61.5 ps as in [23, 29, 30]. At high-statistical measurements (more than ten millions of counts), the best results were obtained with four-term decomposition procedure. Such approach allows us to study nanopores of different sizes, responsible for o-Ps decaying. Each PALS spectrum was processed multiply owing to slight changes in the number of final channels, annihilation background, and time shift of the 0-th channel. In such a manner, we obtained fitting parameters (positron lifetimes τ_1, τ_2, τ_3, τ_4 and corresponding unity-normalized intensities I_1, I_2, I_3, I_4), which correspond to annihilation of positrons in the samples of interest.

In the all three approaches with using a well-developed formalism for two-state positron trapping model [21, 31, 32], the following parameters describing positron

lifetime spectra can be calculated according to Eqs. (1–3):

$$\kappa_d = \frac{I_2}{I_1}\left(\frac{1}{\tau_b} - \frac{1}{\tau_2}\right), \tag{1}$$

$$\tau_b = \frac{I_1 + I_2}{\frac{I_1}{\tau_1} + \frac{I_2}{\tau_2}}, \tag{2}$$

$$\tau_{av.} = \frac{\tau_1 I_1 + \tau_2 I_2}{I_1 + I_2}, \tag{3}$$

where κ_d is positron trapping rate in defect, τ_b—positron lifetime in defect-free bulk, and $\tau_{av.}$—average positron lifetime. In addition, the difference $(\tau_2 - \tau_b)$ can be accepted as a size measure of extended defects where positrons are trapped in terms of equivalent number of monovacancies, as well as the τ_2/τ_b ratio represents the nature of these defects.

3 Results and Discussion

3.1 *Water–adsorption Processes in Nanostructured $MgAl_2O_3$ Ceramics Studied by Three-Component Fitting Procedure*

The obtained PALS characteristics for the $MgAl_2O_4$ ceramics sintered at different T_s before and after water-immersion have a peak and region of smooth fading of coincidence counts in time (Fig. 2). Mathematically such curves describe by sum of exponential functions with different indexes (inversed to lifetimes).

As has been shown [21, 28], at three-component fitting procedure, the shortest (lifetime τ_1 and intensity I_1) and middle (lifetime τ_2 and intensity I_2) PALS components were ascribed to positron trapping modes. By accepting two-state positron trapping model [32], the longer τ_2 lifetime can be treated as defect-related one; these positron trapping defects being located near grain boundaries [33].

Obtained fitting parameters and positron trapping modes for initial and water-immersed $MgAl_2O_4$ ceramics are shown in Tables 1 and 2, respectively. The radii R_3 of spherical nanopores (given in Table 2) were calculated using of o-Ps-related τ_3 lifetime in known Tao-Eldrup model [34, 35]:

$$\tau_{o-Ps} = \left[2\left(1 - \frac{R}{R + \Delta R} + \frac{1}{2\pi}\sin\left(\frac{2\pi R}{R + \Delta R}\right)\right) + 0.007\right]^{-1} \tag{4}$$

where ΔR is empirically derived parameter ($\Delta R \approx 0.1656$ nm for polymers [18]), which describes effective thickness of the electron layer responsible for the "pick-off" annihilation of *o-Ps* in a hole.

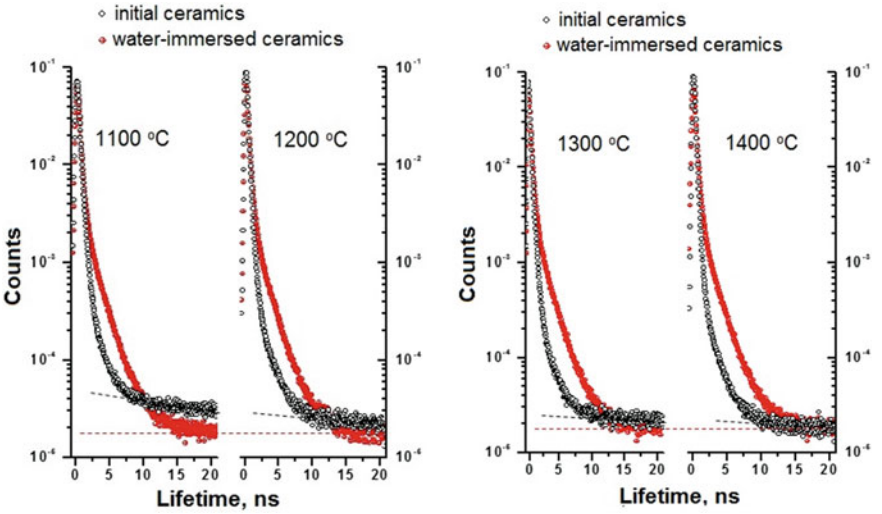

Fig. 2 Positron lifetime spectra for initial and water-immersed $MgAl_2O_4$ ceramics sintered at different T_s [28]

Table 1 Fitting parameters for initial and water-immersed $MgAl_2O_4$ ceramics mathematically treated within three-component procedure [21]

T_s, °C	Sample pre-history	τ_1, ns	I_1, a.u	τ_2, ns	I_2, a.u	τ_3, ns	I_3, a.u
1100	Initial	0.24	0.68	0.50	0.30	2.59	0.02
	Water-immersed	0.24	0.56	0.50	0.29	1.88	0.15
1200	Initial	0.23	0.70	0.47	0.28	2.39	0.02
	Water-immersed	0.22	0.54	0.45	0.34	1.87	0.12
1300	Initial	0.22	0.72	0.44	0.26	2.19	0.02
	Water-immersed	0.22	0.54	0.46	0.32	1.88	0.15
1400	Initial	0.19	0.76	0.36	0.22	1.90	0.02
	Water-immersed	0.21	0.56	0.43	0.32	1.94	0.12

As has been shown early [21–24] and above, the first component of PALS spectra with lifetime τ_1 and intensity I_1 as well as the second component with lifetime τ_2 and intensity I_2 are related to positron trapping modes. The lifetime τ_2 reflects positron trapping on defects located near grain boundaries on ceramic materials.

In initial ceramic samples obtained at different T_s, the shortest τ_1 and middle τ_2 positron lifetimes and intensities I_1 and I_2 reduced with rises of sintering temperature (see Table 1 and Fig. 3). In spate of structural distinction of ceramics sintered at different T_s, positrons are trapped in defects with the same rate of $\kappa_d = 0.60\ ns^{-1}$ (Table 2). The radii R_3 of spherical nanopores (given in Fig. 3) were calculated using τ_3 lifetimes in Tao-Eldrup model.

Table 2 Positron trapping modes for initial and water-immersed $MgAl_2O_4$ ceramics mathematically treated within three-component procedure [21]

T_s, °C	Sample pre-history	$\tau_{av.}$, ns	τ_b, ns	κ_d, ns^{-1}	τ_2- τ_b, ns	τ_2/τ_b	R_3, nm
1100	Initial	0.32	0.28	0.60	0.21	1.7	0.338
	Water-immersed	0.33	0.29	0.70	0.21	1.7	0.276
1200	Initial	0.30	0.27	0.60	0.20	1.7	0.322
	Water-immersed	0.31	0.27	0.90	0.18	1.7	0.275
1300	Initial	0.27	0.25	0.60	0.19	1.7	0.305
	Water-immersed	0.31	0.27	0.90	0.19	1.7	0.276
1400	Initial	0.24	0.21	0.60	0.15	1.7	0.278
	Water-immersed	0.29	0.26	0.90	0.17	1.7	0.282

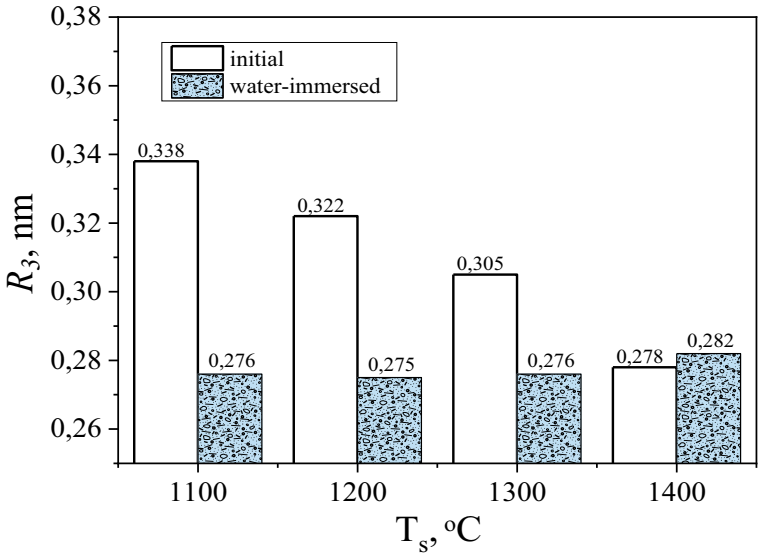

Fig. 3 Nanopore radii R_3 in $MgAl_2O_4$ ceramics sintered at 1100–1400 °C changed in water–adsorption cycles

The third PALS component with lifetime τ_3 is related with o-Ps decaying. In initial ceramic samples, this lifetime reduces from 2.6 to 1.9 ns with T_s, but intensity I_3 is closed to 0.02. In water-adsorbed ceramics, lifetime τ_3 is closed to 1,84 ns, while τ_3 ~ 1.88 ns is related to o-Ps "pick-off" decaying in water at 20 °C. In all cases, intensity I_3 rises from 2% to 0.12–0.15 a.u. testifying large amount of adsorbed water in ceramic samples. This change is accompanied by reduced in parameters of the first PALS component, but parameters of the second component are without changes.

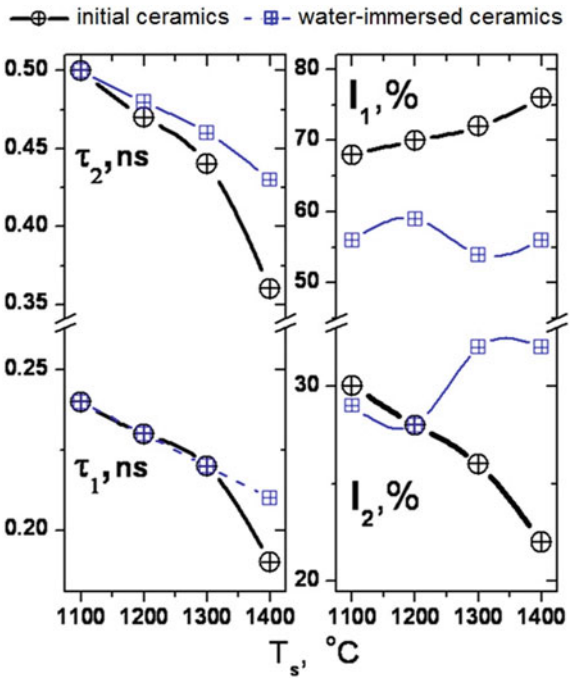

Fig. 4 Changes in lifetime components in dependence on sintering temperature of $MgAl_2O_4$ ceramics [28]

3.2 *Water–Adsorption Processes in Nanostructured $MgAl_2O_3$ Ceramics Studied by Three-Component Fitting Procedure with Fixation of the Lifetimes*

To study more considerable changes in positron trapping in the $MgAl_2O_4$ ceramics caused by absorbed water, the new algorithm is needed to treatment of PALS data [24]. This task can be permitted due to fixation of τ_1 and τ_2 parameters because adsorbed water not changes structure of spinel ceramics.

As was described above, the lifetime τ_2 is related to extended defects near grain boundaries in ceramic materials. Positrons are trapped in the same defects in $MgAl_2O_4$ ceramics independent on amount of adsorbed water by their nanopores. So, the first and second positron lifetimes (τ_1 and τ_2) can be considered near constant. Therefore, all changes in fitting parameters of these components will be reflected in intensities I_1 and I_2. The third lifetime τ_3 is non-fixed (see Table 3). Treatment of experimental PALS data was carried out at fixed lifetimes ($\tau_1 = 0.17$–0.2 ns and $\tau_2 = 0.36$–0.38 ns). At that, the best FIT parameters were obtained at constant lifetimes $\tau_1 = 0.17$ ns and $\tau_2 = 0.37$ ns [24].

The I_1 and I_2 intensities are changed dependently from amount of adsorbed water in $MgAl_2O_4$ ceramics. Thus, rising of *RH* from 25 to 98% results in reducing of intensity I_1 and increasing of intensity I_2. The changes of RH from 98 to 25% reflect inverse to previously described transformation in I_1 and I_2 intensities (Table 3). The

Table 3 PALS characteristics for $MgAl_2O_4$ ceramics sintered at 1300 °C (RH = 25%–60%–98%–60%–25%)

RH, %	Fitting prameters						Positron trapping modes				
	τ_1, ns	I_1, a.u	τ_2, ns	I_2, a.u	τ_3, ns	I_3, a.u	$\tau_{av.}$, ns	τ_b, ns	κ_d, ns^{-1}	τ_2-τ_b, ns	τ_2/τ_b
25	0.18	0.79	0.38	0.20	2.37	0.01	0.22	0.20	0.59	0.18	1.89
60	0.18	0.78	0.38	0.21	2.55	0.01	0.22	0.20	0.62	0.18	1.87
98	0.18	0.76	0.38	0.23	2.27	0.01	0.22	0.20	0.67	0.18	1.86
60	0.18	0.77	0.38	0.22	2.26	0.01	0.22	0.20	0.64	0.18	1.87
25	0.18	0.78	0.38	0.21	2.21	0.01	0.22	0.20	0.61	0.18	1.88

positron trapping in water-immersed defects related to the second component is more intensive. The lifetimes τ_3 are near 2.3–2.8 ns. The input of this component is not changed, and intensity is near 1% [36].

In contrast, most significant changes in positron trapping in $MgAl_2O_4$ ceramics caused by water-sorption reflect in positron trapping rate in defect κ_d (Fig. 5). Thus, the water-sorption effect in the studied spinel ceramics is accumulated in non-direct trapping κ_d parameter [24].

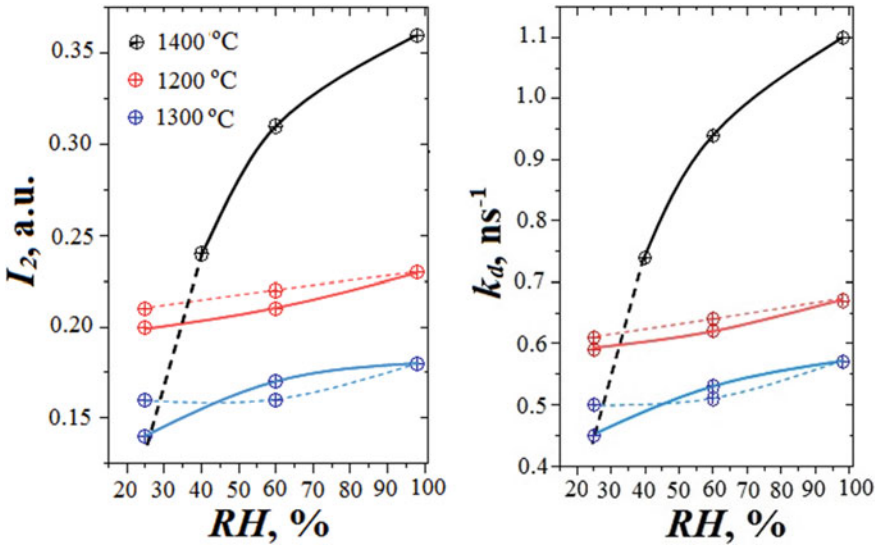

Fig. 5 Dependences of positron intensity I_2 and positron trapping rate κ_d on relative humidity in adsorption–desorption cycles for the $MgAl_2O_4$ ceramics sintered at different T_s [28]

3.3 *Water–Adsorption Processes in Nanostructured $MgAl_2O_3$ Ceramics Studied by Four-Component Fitting Procedure*

Fitting parameters obtained within four-component treatment of the reconstructed PALS spectra of initial and water vapor $MgAl_2O_4$ ceramics sintered at 1100–1400 °C are gathered in Table 4. It is established that τ_1 lifetime in the dried ceramics decreases with T_s, while I_1 intensity increases in respect to amount of main spinel phase like in [32]. Positrons are trapped more strongly in ceramics prepared at lower T_s, as reflected in the values of the second component of the reconstructed PALS spectra. As it follows from Table 4, the numerical values of this component (τ_2 and I_2) decrease with T_s.

As it follows from Table 5, the calculated values of positron trapping modes in

Table 4 Fitting parameters for $MgAl_2O_4$ ceramics sintered at different T_s obtained at four-component decomposition procedure [23]

T_s, °C	Sample pre-history	τ_1, ns	I_1, a.u	τ_2, ns	I_2, a.u	τ_3, ns	I_3, a.u	τ_4, ns	I_4, a.u
1100	Initial	0.169	0.68	0.462	0.28	2.240	0.017	70.14	0.025
	Water vapor	0.170	0.66	0.483	0.28	1.820	0.044	53.05	0.009
1200	Initial	0.164	0.73	0.443	0.24	2.347	0.011	70.51	0.020
	Water vapor	0.160	0.64	0.426	0.31	2.047	0.038	58.67	0.004
1300	Initial	0.155	0.82	0.414	0.16	2.426	0.008	68.74	0.014
	Water vapor	0.161	0.76	0.400	0.21	2.619	0.018	58.33	0.007
1400	Initial	0.152	0.88	0.388	0.11	2.504	0.007	62.32	0.008
	Water vapor	0.160	0.77	0.409	0.20	2.562	0.022	57.35	0.006

Table 5 Positron trapping modes and radii of nanopores determined from four-component fitting procedure for $MgAl_2O_4$ ceramics sintered at different T_s [23]

T_s, °C	Sample pre-history	Positron trapping modes					Radii of nanopores	
		$\tau_{av.}$, ns	τ_b, ns	κ_d, ns^{-1}	$\tau_2 - \tau_b$, ns	τ_2/τ_b	R_3, nm	R_4, nm
1100	Initial	0.289	0.215	1.260	0.349	2.627	0.309	1.844
	Water vapor	0.333	0.225	1.442	0.440	2.953	0.271	1.539
1200	Initial	0.257	0.199	1.074	0.327	2.643	0.319	1.852
	Water vapor	0.321	0.224	1.525	0.379	2.691	0.293	1.636
1300	Initial	0.176	0.764	0.334	2.901	0.176	0.325	1.818
	Water vapor	0.193	1.032	0.382	2.978	0.193	0.340	1.630
1400	Initial	0.195	0.166	0.544	0.349	3.108	0.331	1.701
	Water vapor	0.263	0.192	1.039	0.430	3.241	0.335	1.613

$MgAl_2O_4$ ceramics (average positron lifetime $\tau_{av.}$, bulk positron lifetimes in defect-free samples τ_b and positron trapping rates in defects κ_d) are decreased with sintering temperature T_s. These parameters are in good agreements with amount of additional MgO and Al_2O_3 phases in the ceramics [32].

At the same time, the principal water–vapor sorption processes in the studied $MgAl_2O_4$ ceramics sintered at 1100–1400 °C occur to be mostly determined by o-Ps related components in the PALS spectra reconstructed through four-term fitting procedure. As it was shown earlier [24, 29], the corresponding long-lived lifetimes τ_3 and τ_4 reflect sizes of nanopores, and their intensities I_3 and I_4 are directly related to the number of these nanopores.

So, in the initial $MgAl_2O_4$ ceramics sintered at 1100–1400 °C, the lifetime τ_3 increases with T_s, while intensity I_3 decreases (Table 4). These changes are due to the increase in the size of small nanopores with radius R_3, and their reduction is caused by increasing contact between grains. The lifetime τ_4 and intensity I_4 naturally decrease with T_s, indicating reduction in size and number of nanopores with radius R_4. The radii R_3 and R_4 of spherical nanopores (given in Table 5) were calculated using τ_3 and τ_4 lifetimes in Tao-Eldrup model. It is shown that radius of nanopores R_3 increases from 0.309 to 0.331 nm, and R_4 remains nearly at the same level (~1.8 nm) in the initially dried ceramics sintered at 1100–1400 °C (Fig. 6).

Preferential decreasing of the lifetime τ_2 in water vapor $MgAl_2O_4$ ceramics and increasing of their intensity I_2 demonstrate intensification of positron trapping in defects near grain boundaries filled with water. Thus, the water–adsorption processes in $MgAl_2O_4$ ceramics are accompanied by fragmentation of positron trapping sites near grain boundaries [23].

Water–vapor sorption processes in the studied ceramics result in essential evolution of third and fourth o-Ps-related components. The intensity I_3 increases in all initial samples after water–vapor exposure, thus confirming o-Ps annihilation in water-filled nanopores through a “bubble” mechanism (with corresponding o-Ps lifetime close to 1.8 ns) [37–39]. At the same time, the lifetime τ_3 decreases in more defective ceramics sintered at 1100 and 1200 °C, but increases in more perfect ceramics sintered at 1300 °C and 1400 °C.

Other mechanism of water–vapor sorption processes similar to one reported in [40] is realized in the studied $MgAl_2O_4$ ceramics through fourth component of the PAL spectra. Unlike the third component, the intensity I_4 decreases in water–vapor exposure ceramics samples. Since this intensity does not drop to zero being within 0.4–0.9% domain, it should be assumed that there exists a fraction of closed nanopores, where o-Ps are trapped [29].

4 Conclusions

Peculiarities of water–adsorption processes in nanostructured humidity-sensitive $MgAl_2O_4$ ceramics studied by positron annihilation lifetime at three- and four-component fitting procedures were generalized. The mathematical treatment of

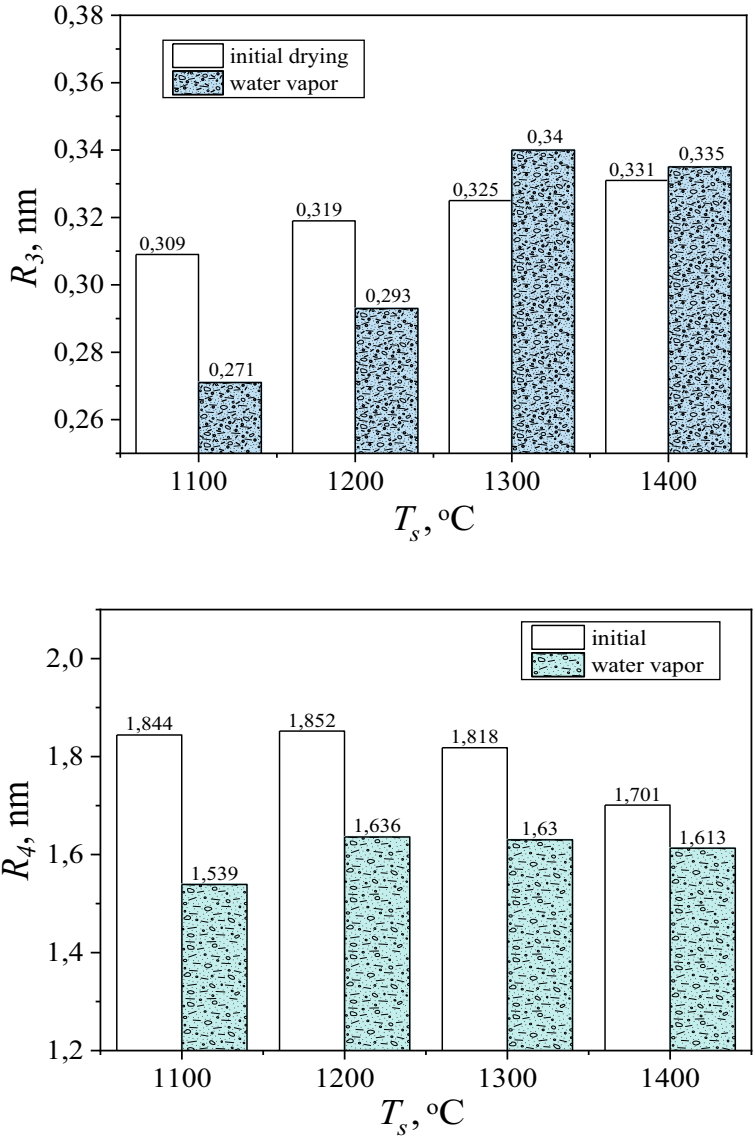

Fig. 6 Nanopore radii R_3 and R_4 in $MgAl_2O_4$ ceramics sintered at 1100–1400 °C changed in water–adsorption cycle

experimental PALS data at constant values of reduced bulk and defect-related lifetimes allows to refine the most significant changes caused by absorbed water in the functional ceramics.

It is shown that positrons are trapped more strongly in the ceramics obtained at lower T_s, which was reflected in the second component of the four-term decomposed PALS spectra. The positron trapping in defects occurs more efficiently in water-immersed ceramics due to increase in positron trapping rate of extended defects. The more perfect structure of ceramics, the more considerable changes occur in the water-absorbing pores.

The third and fourth longest-lived components in PALS spectra are due to annihilation of o-Ps atoms in the nanopores, the corresponding radii being calculated from τ_3 and τ_4 lifetimes using known Tao-Eldrup model. The Ps annihilation in nanopores with adsorbed water vapor is shown to occur via two mechanisms: o-Ps decaying in nanopores including "pick-off" annihilation in the "bubbles" of liquid water and o-Ps trapping in free volume of nanopores with physisorbed water molecules at the pore walls. The water vapor modifies defects in ceramics located near grain boundaries, and this process accompanied by void fragmentation at water–adsorption.

The fixation of all water-dependent positron trapping inputs allows to refine the most significant changes in positron trapping rate of extended defects located near grain boundaries. The water–adsorption processes in $MgAl_2O_4$ ceramics leads to corresponding increase in positron trapping rates of extended defects located near grain boundaries.

Acknowledgements H.K. thanks to Ministry of Education and Science of Ukraine for support, Prof. O. Shpotyuk for discussion, Dr. I. Hadzaman for sample preparation and Dr. A. Ingram for assistance in PALS experiment.

References

1. Gusmano G, Montesperelli G, Traversa E, Bearzotti A, Petrocco G, d'Amico A, Di Natal, C (1992) Magnesium aluminium spinel thin film as a humidity sensor. Sens Actu B Chem 7(1–3):460–463. https://www.sciencedirect.com/science/article/abs/pii/092540059280344W
2. Zhao X, Ren X, Sun C, Zhang X, Si Y, Yan C, Xu J, Xue D (2008) Morphology evolution at nano-to micro-scale. Funct Mater Lett 1(03):167–172. https://www.worldscientific.com/doi/abs/10.1142/S1793604708000393
3. Li JG, Ikegami T, Lee JH, Mori T (2000) Fabrication of translucent magnesium aluminum spinel ceramics. J Am Ceram Soc 83(11):2866–2868. https://ceramics.onlinelibrary.wiley.com/doi/abs/10.1111/j.1151-2916.2000.tb01648.x
4. Laobuthee, A, Wongkasemjit S, Traversa E, Laine RM (2000) $MgAl_2O_4$ spinel powders from oxide one pot synthesis (OOPS) process for ceramic humidity sensors. J Eur Ceram Soc 20(2):91–97. https://www.sciencedirect.com/science/article/abs/pii/S0955221999001533
5. Mordekovitz Y, Shoval Y, Froumin N, Hayun S (2020) Effect of structure and composition of non-stoichiometry magnesium aluminate spinel on water adsorption. Materials 13(14):3195. https://www.mdpi.com/1996-1944/13/14/3195
6. Wang Z, Chang CL, Zhao X, Qian W, Zhang X, Xie Z, Hwang B-H, Hu C, Shen J, Hui R (2009) $MgAl_2O_4$-based humidity-sensing material for potential application in PEM fuel cells.

J Power Sources 190(2):351–355. https://www.sciencedirect.com/science/article/abs/pii/S037877530801762X
7. Shah J, Kotnala RK (2012) Humidity sensing exclusively by physisorption of water vapors on magnesium ferrite. Sens Act B Chem 171:832–837. https://www.sciencedirect.com/science/article/abs/pii/S0925400512005497
8. Klym H, Ingram A, Shpotyuk O, Hadzaman I (2012) Water-sorption processes in nanostructured ceramics for sensor electronics studied with positron annihilation instruments. In: 28th International conference on microelectronics (MIEL), pp 155–158. https://doi.org/10.1109/MIEL.2012.6222821
9. Henninger SK, Schmidt FP, Henning HM (2010) Water adsorption characteristics of novel materials for heat transformation applications. Appl Therm Eng 30(13):1692–1702. https://www.sciencedirect.com/science/article/abs/pii/S1359431110001389
10. Klym H, Ingram A, Shpotyuk O, Hadzaman I, Chalyy D (2018) Water-sorption effects near grain boundaries in modified MgO-Al_2O_3 ceramics tested with positron-positronium trapping algorithm. Acta Phys Pol A 133(4):864–868. https://doi.org/10.12693/APhysPolA.133.864
11. Klym H, Ingram A, Hadzaman I, Karbovnyk I, Vasylchyshyn I, Popov AI (2019) Nanoporous characterization of modified humidity-sensitive MgO-Al_2O_3 ceramics by positron annihilation lifetime spectroscopy method. IOP Conf Ser Mater Sci Eng 503(1):012019. https://iopscience.iop.org/article/10.1088/1757-899X/503/1/012019/meta
12. Shpotyuk O, Balitska V, Brunner M, Hadzaman I, Klym H (2015) Thermally-induced electronic relaxation in structurally-modified $Cu_{0.1}Ni_{0.8}Co_{0.2}Mn_{1.9}O_4$ spinel ceramics. Phys B Condens Matter 459:116–121. https://www.sciencedirect.com/science/article/abs/pii/S0921452614008576
13. Karbovnyk I, Bolesta I, Rovetskii I, Velgosh S, Klym H (2014) Studies of CdI_2-Bi_3 microstructures with optical methods, atomic force microscopy and positron annihilation spectroscopy. Mater Sci Poland 32(3):391–395. https://link.springer.com/article/10.2478/s13536-014-0215-z
14. Bondarchuk A, Shpotyuk O, Glot A, Klym H (2012) Current saturation in In_2O_3-SrO ceramics: a role of oxidizing atmosphere. Rev Mex Fís 58(4):313–316. http://www.scielo.org.mx/scielo.php?script=sci_arttext&pid=S0035-001X2012000400005
15. Shpotyuk O, Brunner M, Hadzaman I, Balitska V, Klym H (2016) Analytical description of degradation-relaxation transformations in nanoinhomogeneous spinel ceramics. Nanoscale Res Lett 11(1):499. https://link.springer.com/article/10.1186/s11671-016-1722-0
16. Klym H, Hadzaman I, Shpotyuk O, Fu Q, Luo W, Deng J (2013) Integrated thick-film p-i-p^+ structures based on spinel ceramics. Solid State Phenom 200:156–161. https://www.scientific.net/ssp.200.156
17. Vakiv M, Hadzaman I, Klym H, Shpotyuk O, Brunner M (2011) Multifunctional thick-film structures based on spinel ceramics for environment sensors. J Phys Conf Ser 289(1):012011. https://iopscience.iop.org/article/10.1088/1742-6596/289/1/012011/meta
18. Karbovnyk I, Olenych I, Aksimentyeva O, Klym H, Dzendzelyuk O, Olenych Y, Hrushetska O (2016) Effect of radiation on the electrical properties of PEDOT-based nanocomposites. Nanoscale Res Lett 11(1):84. https://link.springer.com/article/10.1186/s11671-016-1293-0
19. Karbovnyk I, Collins J, Bolesta I, Stelmashchuk A, Kolkevych A, Velupillai S, Klym H, Fedyshyn O, Tymoshyk S, Kolych I (2015) Random nanostructured metallic films for environmental monitoring and optical sensing: experimental and computational studies. Nanoscale Res Lett 10(1):1–5. https://nanoscalereslett.springeropen.com/articles/10.1186/s11671-015-0855-x
20. Krause-Rehberg R, Leipner HS (1999) Positron annihilation in semiconductors. In: Defect studies. Springer, Berlin-Heidelberg-New York, p 378
21. Klym H, Ingram A, Shpotyuk O, Filipecki J, Hadzaman I (2007) Extended positron-trapping defects in insulating $MgAl_2O_4$ spinel-type ceramics. Physica Status Solidi c 4(3):715–718. https://onlinelibrary.wiley.com/doi/abs/10.1002/pssc.200673735
22. Jean YC, Mallon PE, Schrader DM (2003) Principles and application of positron and positronium chemistry. Word Scientific, Singapore

23. Klym H, Ingram A, Shpotyuk O, Hadzaman I, Solntsev V (2016) Water-vapor sorption processes in nanoporous MgO-Al_2O_3 ceramics: the PAL spectroscopy study. Nanoscale Res Lett 11(1):1. https://doi.org/10.1186/s11671-016-1352-6
24. Filipecki J, Ingram A, Klym H, Shpotyuk O, Vakiv M (2007) Water-sensitive positron-trapping modes in nanoporous magnesium aluminate ceramics. J Phys Conf Ser 79(1):012015. https://doi.org/10.1088/1742-6596/79/1/012015
25. Klym HI, Ivanusa AI, Kostiv YuM, Chalyy DO, Tkachuk TI, Dunets RB, Vasylchyshyn II (2017) Methodology and algorithm of multicomponent analysis of positron annihilation spectra for nanostructured functional materials. J Nano- Electron Phys 9(3):03037-1-6. https://doi.org/10.21272/jnep.9(3).03037
26. Shpotyuk O, Filipecki J: Free volume in vitreous chalcogenide semiconductors: possibilities of positron annihilation lifetime study. Wyd-wo WSP w Czestochowie, Czestochowa
27. Kansy J (1996) Microcomputer program for analysis of positron annihilation lifetime spectra. Nucl Instrum Methods Phys Res, Sect A 374(2):235–244
28. Klym H, Dunets R, Ivanusa A, Kostiv Y, Yurchak I (2017) Modified humidity-sensitive ceramics for microelectronics studied by PALS system. In: IEEE First Ukraine conference on electrical and computer engineering (UKRCON), pp 732–735. https://ieeexplore.ieee.org/abstract/document/8100341
29. Golovchak R, Wang Sh, Jain H, Ingram A (2012) Positron annihilation lifetime spectroscopy of nano/macroporous bioactive glasses. J Mater Res 27(19):2561–2567
30. Kobayashi Y, Ito K, Oka T, Hirata K (2007) Positronium chemistry in porous materials. Radiat Phys Chem 76:224–230. https://www.sciencedirect.com/science/article/abs/pii/S0969806X06001496
31. Nambissan PMG, Upadhyay C, Verma HC (2003) Positron lifetime spectroscopic studies of nanocrystalline $ZnFe_2O_4$. J Appl Phys 93:6320. https://aip.scitation.org/doi/abs/10.1063/1.1569973
32. Klym H, Ingram A (2007) Unified model of multichannel positron annihilation in nanoporous magnesium aluminate ceramics. J Phys Conf Ser 79(1):012014. https://iopscience.iop.org/article/10.1088/1742-6596/79/1/012014/meta
33. Klym H, Ingram A, Shpotyuk O, Filipecki J, Hadzaman I (2011). Structural studies of spinel manganite ceramics with positron annihilation lifetime spectroscopy. J Phys Conf Ser 289(1):012010. https://iopscience.iop.org/article/10.1088/1742-6596/289/1/012010/meta
34. Tao SJ (1972) Positronium annihilation in molecular substance. J Chem Phys 56(11):5499–5510. https://doi.org/10.1063/1.1677067
35. Eldrup M, Lightbody D, Sherwood JN (1981) The temperature dependence of positron lifetimes in solid pivalic acid. Chem Phys 63:51–58. https://doi.org/10.1016/0301-0104(81)80307-2
36. Klym H, Ingram A, Shpotyuk O, Hadzaman I, Hotra O, Kostiv Y (2016) Nanostructural free-volume effects in humidity-sensitive MgO-Al_2O_3 ceramics for sensor applications. J Mater Eng Perform 25(3):866–873. https://doi.org/10.1007/s11665-016-1931-9
37. Leifer I, Patro RK (2002) The bubble mechanism for methane transport from the shallow sea bed to the surface: a review and sensitivity study. Cont Shelf Res 22(16): 2409–2428. https://www.sciencedirect.com/science/article/abs/pii/S0278434302000651
38. Ljunggren S, Eriksson JC (1997) The lifetime of a colloid-sized gas bubble in water and the cause of the hydrophobic attraction. Colloids Surfaces A Physicochem Eng Aspects 129:151–155. https://www.sciencedirect.com/science/article/abs/pii/S0927775797000332
39. Grosman A, Ortega C (2005) Nature of capillary condensation and evaporation processes in ordered porous materials. Langmuir 21:10515–10521. https://pubs.acs.org/doi/abs/10.1021/la051030o
40. Dlubek G, Yang Yu, Krause-Rehberg R, Beichel W, Bulut S, Pogodina N, Krossing I, Friedrich Ch (2010) Free volume in imidazolium triflimide ($[C_3MIM][NTf_2]$) ionic liquid from positron lifetime: Amorphous, crystalline, and liquid states. J Chem Phys 133:124502. https://aip.scitation.org/doi/abs/10.1063/1.3487522